SPECTROSCOPY OF POSITRONS FROM HEAVY-ION ATOM COLLISIONS AT COULOMB BARRIER ENERGIES

P. SALABURA[a,c], A. BAŁANDA[c], H. BOKEMEYER[a],

K. SAKAGUCHI[a], K.E. STIEBING[b]

[a]Gesellschaft für Schwerionenforschung mbH
D-64291 Darmstadt, Planckstrasse 1, Germany
[b]Institut für Kernphysik, J. W. Goethe Universität
D-60486, Frankfurt, August-Euler-Str.6, Germany
[c]Institute of Physics, Jagellonian University
Reymonta 4, 30-059 Cracow, Poland

(Received January 24, 1995; revised version received March 13, 1995)

The EPOS experiments at the UNILAC accelerator of GSI are reviewed as an example of the development of positron spectroscopy in heavy-ion collisions. The phenomenon of anomalous lines observed in inclusive positron spectra and in electron-positron sum energy spectra as well as the derivation of background of nuclear and atomic positrons is discussed. The article closes with an outlook on a new generation of the experiments currently started with considerably upgraded instruments.

PACS numbers: 31.50.+w

1. Introduction

Heavy-ion (HI) collisions at Coulomb barrier energies offer a unique opportunity to study electronic behaviour in quasi-atoms at closest internuclear separations of the order of nuclear dimensions. For a short period during the collision of about 10^{-21} s the electric field reaches strengths of $> 10^{19}$ V/m with the consequence that for the innermost electronic orbits the enormous Coulomb force leads to a dramatic increase of their binding energies. In particular, for supercritical quasi-atomic systems with united charges $Z_u = Z_1 + Z_2 \geq Z_c = 173$, the binding energy of the $1s\sigma$-electronic state in the two-center potential of the colliding nuclei exceeds $2m_ec^2$ [1, 2] thus forming a resonance in the negative-energy continuum. If the state is

empty due to prior ionization it can be *spontaneously* filled by an electron from the Dirac sea, there leaving a hole subsequently emitted as a positron by Coulomb repulsion. This is a process of fundamental importance: the physical electronic ground state becomes unstable in the presence of a supercritical charge, with the consequence that the neutral vacuum spontaneously decays into a locally charged vacuum. The search for the spontaneous vacuum decay has initially motivated the experiments on positron spectroscopy in heavy ion collisions at the UNILAC accelerator of the Gesellschaft für Schwerionenforschung (GSI), Darmstadt.

The field was introduced by pioneering theoretical works predicting spontaneous positron emission [3, 4]. These were soon fully developed [2] to the present quasi-atomic (QA) picture when experimental results became accessible with the operation of the UNILAC accelerator in the 70's. A mile stone on the way to experimentally verify the exciting prediction was reached. In fact, many experiments performed at GSI in 1978-85 focused its attention on this question. The predicted strong electronic binding has been explored by studying ionization processes of the innermost atomic shells induced from the fast changing strong Coulomb potential by K-hole production, emission of high energy δ-electrons, quasi-molecular X-ray (MO-X-ray) or characteristic X-ray emission. With sufficiently high QA charge the electronic excitations induced from the fast changing strong Coulomb potential may include the negative-energy continuum states with the electrons then excited to vacant bound states or to positive-energy continuum states. The resulting *dynamically induced or QA positron emission* provides an additional experimental probe to study the structure of superheavy QA's. Although of basically different mechanism, the spontaneous positron emission therein forms a principally undistinguishable component. In Section 2 we discuss to some detail selected experimental results which confirm the basic concept of the QA model.

The harsh nature of the HI collision environment, as well as the small cross section, places stringent demands on an experimental apparatus to safely measure atomic positron production in HI collisions. The spectrometer needs a large detection efficiency for positrons as well as a high discriminative power to cope with small production rates of the order of 10^{-6} per collision for positrons and at the same time large background yields of δ-electrons, γ-rays, X-rays produced with probabilities on the order of 1 per collision. γ-rays and conversion electrons have to be measured simultaneously with the positrons in order to evaluate the nuclear electron-positron pair contribution in the e^+e^- spectra which stems from Internal Pair Conversion (IPC) processes of nuclear transitions. In Section 3 we describe the EPOS (**E**lectron **PO**sitron **S**olenoid) spectrometer [5–8] which comprises the above mentioned requirements by combining a magnetic solenoidal field

for the transport of the electrons and positrons from the target to high resolution Si(Li)-detector systems placed at the focal areas. Another experiment designed by the ORANGE collaboration [9] makes use of a dispersive, large acceptance ORANGE β-spectrometer to reach the above demands.

The experiments performed by the EPOS group became exciting when on top of the smooth continuous QA positron spectra measured in coincidence with quasi-elastic HI collisions of heaviest elements, like U on Cm, narrow line structures around 300 to 400 keV were identified [10, 11]. The widths of the lines on the order of 80 keV were considerably less than what is expected from Doppler broadening of the lines due to high emitter velocities. Similar observations were made independently by the ORANGE collaboration [12, 13]. These lines were tentatively associated with the process of spontaneous positron emission. But this exciting interpretation implies the simultaneous existence of a long-living di-nuclear molecules with life-times of the order of 10^{-20}s just to accomplish the uncertainty relation. Subsequent experiments revealed, that the energies of the positron lines, although different for each individual projectile target combination, were essentially independent from the collision system with the united charge number Z_u varied from 163 to 188. For the spontaneous positron decay, however, it is predicted that the line position varies strongly with Z_u in accordance with the increase of the overcritical $1s\sigma$ binding energy with increasing Z_u. Moreover, for $Z_u < 173$ there is no overcritical binding and a spontaneous positron emission should not exist at all. Section 4 is related to the systematic study of positron lines in inclusive positron spectra as well as to the qualitative description of the continuous part of the spectra by nuclear and QA positron production.

The near constancy of the positron peak energy as well as the apparent inability of explaining the lines with conventional processes suggests an unorthodox phenomenon. An obvious speculation [14, 11, 15, 16] for such a source is the two-body decay into an electron positron pair of a previously undetected neutral object X with a mass around 1.8 MeV/c^2, as derived from the positron lines energies assuming comparable kinetic electron and positron energies and adding the rest energy. In order to test this hypothesis the EPOS experiment was modified to search for coincident electrons as partner of the positrons. These experiments revealed sharp lines in the spectra of the sum E_Σ of the electron and positron kinetic energies [17–20] which were significantly narrower ($\Delta E_\Sigma \sim 25 - 40$keV) than what is expected from a convolution of individual Doppler broadening of the electron and positron energies ($\Delta E_{e+} \sim \Delta E_{e-} \sim 80$keV). This suggests a mutual cancellation of the kinematic shifts (hereon called Doppler shifts, although — if taken strictly — reserved for massless particles) introduced from the high velocity of the emitting HI system around 5 to 10 % of light veloc-

ity. In Section 5 we summarize the results on the electron positron line phenomenon from EPOS together with some of the results obtained independently in the ORANGE experiments [21, 9]. Till today, these lines could not be explained by known processes if not very unconventional scenarios are incorporated. In particular, IPC as a three body decay process does not provide for the respective kinematic to result in narrow lines, nor have singular nuclear transitions been found with sufficient cross sections to explain the line intensities with usual IPC conversion coefficients and usual emission characteristics.

Arrived at this point the hunt for X-objects was open triggering an enormous number of experimental and theoretical studies. To date any additional fundamental particle at this mass range — originally the lines were associated with the illusive axion [22, 23] — is excluded [15, 24]. Composed objects exclusively formed within the particular HI collision environment with sizes exceeding the Compton wave length may still be a hypothetical source of the line but complex scenarios combining known mechanism in an unorthodox way have as well to be considered seriously. Theoretical advise could not be given on a still poor basis of present experimental information on the lines.

With the apparent need for more systematic and statistically improved data to resolve the puzzling line production, a new round of experiments has been started recently with upgraded EPOS and ORANGE spectrometers and the newly constructed APEX setup at the ATLAS accelerator of Argonne National Laboratory. The last section will shortly report on the status of these experiments.

2. Quasiatomic picture of colliding ions

The expression for the total energy of the lowest bound $1s$-state for a hydrogen-like atom as given by the Dirac-Sommerfeld fine-structure formula

$$E_{1s} \simeq m_e c^2 [1 - (Z\alpha)^2]^{1/2} ,$$

becomes imaginary for $Z\alpha > 1$. The electronic energy levels for a nucleus with $Z > 137$ have first been calculated within the Dirac theory in 1945 [25]. The key for these calculations is the assumption of a finite size of the nucleus to remove the singularity in the Coulomb potential at the origin. More exact calculations (*e.g.* [26]) show, that the binding energy even exceeds $2m_e c^2 = 1022$ keV at a critical charge of $Z_c \simeq 173$. Such heavy species do not exist statically in nature but are transiently accessible experimentally in heavy-ion collisions at projectile energies sufficiently high to balance the repulsion of the Coulomb potential but still below the onset of nuclear reactions. For a short period of 10^{-21} s when the two colliding nuclei approach internuclear

distances $R(t)$ of a few fm, they form an united charge center for the atomic electrons. Such a situation is schematically shown in Fig. 1 as the example of central uranium on uranium collisions ($Z_u = Z_1 + Z_2 = 184$) at a projectile energy of 5.9 MeV/u. The time evolution of $R(t)$, shown in Fig. 1, is calculated assuming classical ion trajectories according to a point charge Coulomb potential. The actual formation of a superheavy "quasi-atom" depends on the fulfillment of adiabacity conditions: the inner-shell electron velocity v_e has to be larger than the projectile velocity v_p and the evolution time of the electronic orbit has to be shorter than the time for passage, such that electron motion adiabatically adjusts to the fast changing two-center Coulomb potential. Indeed, as seen from given example with $v_p = 0.1c$, for the uranium K-shell electron, typical values $v_e \simeq 0.6c$ and $r_{1s} \simeq 800$ fm indicate that such condition can well be reached in very heavy ion collisions.

The evolution of QA electronic orbits can fully be calculated within the framework of the time-dependent two-center Dirac equation (TCD) assuming the ions moving along elastic trajectories. Fig. 1 (lower part) shows the resulting binding energy of the three innermost electronic orbits as a function of $R(t)$. The binding energies increase rapidly with decreasing $R(t)$. For the $1s$-state the situation becomes overcritical when the binding energy reaches $-2mc^2$, thus providing sufficient energy to spontaneously form an electron positron pair with the positron emitted while the electron remains captured assuming the $1s$ shell was empty by prior ionization. Besides this exciting static aspect the time evolution of the system leads to a dynamic coupling between the QA levels and the positive and negative energy continuum resulting into electronic excitations: electrons from the negative energy continuum can be excited to vacant bound states and to the positive energy continuum states; the latter process is known as $\delta-$ electron emission. The remaining holes in the negative energy continuum result in *dynamically induced QA positron emission.* Induced positron emission is characterized by continuous, bell-shaped energy distributions peaked around 500 keV reflecting the intrinsic momentum distributions of the initial QA states as well as the repulsion of the positron from the QA potential.

The time-dependent TCD equation is solved in the nucleus-nucleus center-of-mass frame (CMS) for an explicitly time dependent internuclear separation $R(t)$:

$$i\hbar\frac{\partial}{\partial t}\Phi_i(t) = H_{\mathrm{TCD}}(R(t))\Phi_i(t)$$

with $H_{\mathrm{TCD}}(R(t))$ the two-center Dirac Hamiltonian. The wave function $\Phi_i(t)$ can be expanded in a complete set of quasimolecular basis functions

$$\Phi_i(t) = \sum_k a_{ik}\phi_k(R(t))\mathrm{e}^{-i\chi_k(t)}\,.$$

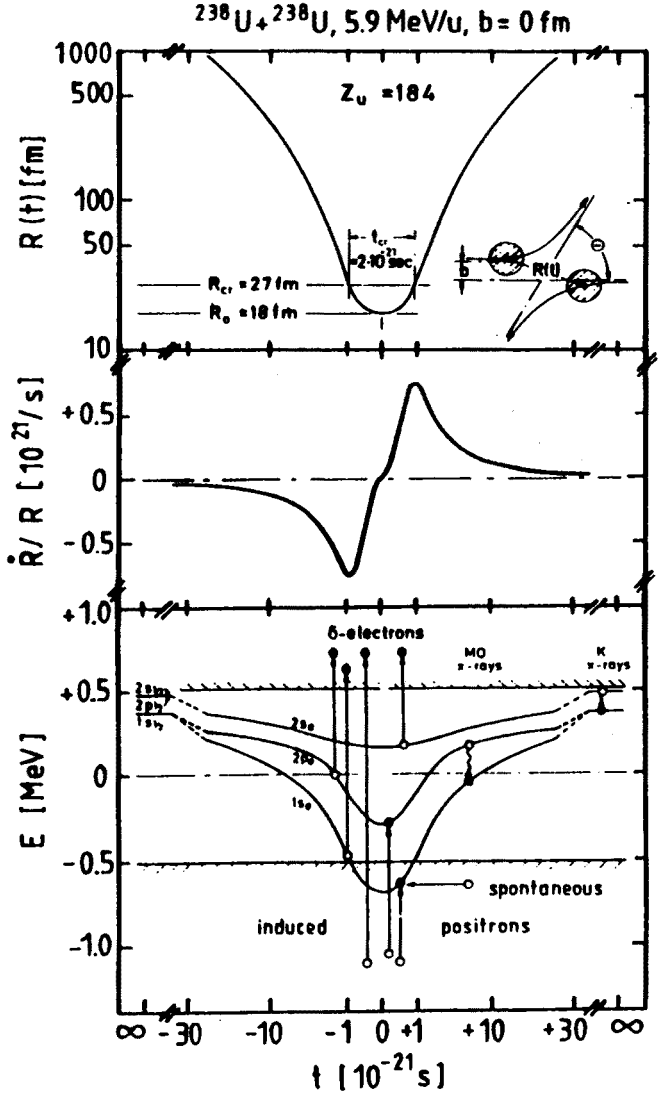

Fig. 1. Time evolution of the internuclear distance $R(t)$ (top) the logarithmic time derivative of the internuclear distance $\dot{R}/R$ (middlepart) and electron binding energies in U+U collisions (bottom). Various excitation processes are depicted: dynamic and spontaneous positron production as well as δ-electron emission.

$\sum$ indicates a summation over bound states and integration over positive and negative energy continuum states. $\phi_i(R(t))$ are solutions of the static TCD equation to be evaluated for each value $R(t)$. The labels i, k stand for the quantum numbers of the total angular momentum j of the QA electronic

state and its projection m_j along the internuclear axis [27]. The phase factor $\chi_k(t)$ is a time-integrated expectation value of H_{TCD} :

$$\chi_k(t) = \frac{1}{\hbar} \int_{-\infty}^{t} dt' \langle \phi_k(R(t')) \mid H_{\mathrm{TCD}}(R(t')) \mid \phi_k(R(t')) \rangle \equiv \frac{1}{\hbar} \int_{-\infty}^{t} dt' E_k(t') .$$

Inserting the above expansion of Φ_i into the time-dependent TCD equation gives the following infinite set of coupled differential equations

$$\frac{\partial}{\partial t} a_{ik}(t) = \sum_{j \neq k} a_{ij}(t) \left\langle \phi_k \left| \frac{\partial}{\partial t} + \frac{i}{\hbar} H_{\mathrm{TCD}} \right| \phi_j \right\rangle \times \mathrm{e}^{-i(\chi_k - \chi_j)} ,$$

which in first order time-dependent perturbation theory can be integrated formally assuming a singularly occupied initial state characterized by $a_i = 1$ and $a_j = 0$ for $j \neq i$ to:

$$a_f(t = \infty) = \int_{-\infty}^{+\infty} dt \left\langle \phi_f \left| \frac{\partial}{\partial t} \right| \phi_i \right\rangle \mathrm{e}^{-i(E_f - E_i)} ,$$

but otherwise has to be solved by numerical integration in a truncated set of basis states. The time derivative operator, responsible for the dynamic couplings can be expressed in the coordinates of the rotating internuclear axis according

$$\frac{\partial}{\partial t} = \dot{R} \frac{\partial}{\partial R} + \dot{\theta} \frac{\partial}{\partial \theta} .$$

The radial coupling term only couples states of same spin j and spin projection m_j, while the rotational coupling term involves states whose total spin projections differ by one unit. Rotational coupling decreases for small values of R and totally vanishes for s-states. Due to the strong binding, the innermost electron wave functions are strongly localized near the origin of the two-center potential with $\sqrt{< r^2_{1s\sigma} >} \approx 100$ fm [28], with the consequence that rotational coupling can be neglected in superheavy systems. The radial coupling matrix element canbe calculated using the Hellmann-Feymann operator equivalence

$$\left\langle \phi_f \left| \frac{\partial}{\partial R} \right| \phi_i \right\rangle = \frac{1}{E_i - E_f} \left\langle \phi_f \left| \frac{\partial H_{\mathrm{TDC}}}{\partial R} \right| \phi_i \right\rangle ,$$

with $i \neq j$.

Introducing in addition the monopole approximation for the two-center Coulomb potential, the ionization amplitude can be analytically expressed

[29–31]. A general form with initial and final states i and f including positron emission can be found in [32]:

$$a(E_f) = \frac{d(E_i, E_f, Z_u)}{E_f - E_i} \int_{-\infty}^{t} dt \frac{\dot{R}}{R} \exp\left\{ i(E_f - E_i)\frac{t}{\hbar} \right\} .$$

This first order formula identifies the logarithmic derivative $\dot{R}/R$ of the internuclear distance as the driving force for QA transitions. $d\left(E_i, E_f, Z_{ua}\right)$ contains the radial part of the QA wave functions which can be expressed by the electronic densities $\rho\left(r, R\right)$ at their origin r=0:

$$d\left(E_i, E_f, Z_u\right) = \frac{1}{12} Z_u e^2 \left[1 - \frac{2}{15} \left(\frac{Z_u e^2}{\hbar c} \right)^2 \right] \left[\rho_f\left(0, R\right) R^2 \rho_i\left(0, R\right) R^2 \right]$$

The characteristic dispersion-like dependence of $\dot{R}/R$ on the collision time shown in Fig. 1 suggests the existence of a critical time [31, 30] expressed by

$$\tau_0 = \frac{1}{v_1} \left[b - a\cos^{-1}\left(\frac{a}{R_o - a} \right) + \pi a \right] = \frac{1}{v_1} \left[b + a\left(\pi - \tan^{-1}\frac{b}{a} \right) \right]$$

with impact parameter $b = a\sqrt{\epsilon^2 - 1}$, the distance of closest approach

$$2a = \frac{Z_1 Z_2 e^2}{E_{CM}} = 1.44\text{fm MeV} \frac{A_1 + A_2}{A_1 A_2} \frac{Z_1 Z_2}{E_1/A_1}$$

and excentricity $\epsilon = (R_o - a)/a = 1/\sin(\theta_{cm}/2)$. For forward collisions with $\epsilon \ll 1$, τ_0 can be reduced to

$$\hat{t} \simeq \frac{a}{v_1} \left(\epsilon + 1.6 + \frac{0.449}{\epsilon} \right) .$$

$\hat{t}$ expresses the time distance between the two extrema of $\dot{R}/R$.

$$\frac{\dot{R}}{R} \simeq \frac{\kappa t}{t^2 + \hat{t}^2} \quad \text{with} \quad \kappa = 1 + 0.174/\epsilon .$$

Reducing τ_0 further leads to a characteristic propagation time

$$t_0 \simeq \frac{R_{\min}}{v_1} \quad \text{with} \quad R_{\min} = a + \sqrt{a^2 + b^2} = a(\epsilon + 1) ,$$

the internuclear distance at the turning point of a trajectory with impact parameter b. Using either of these expressions very useful scaling relations have been derived for the different QA excitations [29, 30].

For example, an useful expression to analytically describe the principle spectral shape of δ-electron emission can be extracted [31]:

$$\frac{dP_{e^-}}{dE_{e^-}} \approx \frac{P_0 \kappa}{(E_{e^-} - E_b)^2} \exp\left[-\frac{2\hat{t}}{\hbar}(E_{e^-} - E_b)\right],$$

with P_0 and E_b fit parameters where E_b has the meaning of effective binding energies, E_{e^-} is the kinetic electron energy. Using τ_0 similar approximation was obtained [30] for the total δ-electron emission probability:

$$\frac{dP_{e^-}}{dE_{e^-}} \approx \pi^2 d_0^2 \left(\frac{mc^2}{E_{e^-}}\right)^{\gamma} \exp\left[-\frac{2\tau_0(E_{e^-} - E_{1s\sigma}(R_{\min}))}{\hbar}\right].$$

The quantities d_0 and γ are given in [29]. Integrating the δ-electron emission probability originating from the $1_{s\sigma}$-state over the final continuum states leads to the K-hole production probability:

$$P_{1s\sigma}(R_{\min}) = \tfrac{1}{2} D(Z_u) \exp\left[\frac{2\tau_0}{\hbar} E_{1s\sigma}(R_{\min})\right]$$

with

$$D(Z_u) = 1.2 + 0.054(Z - 158) - 0.000015(Z - 158)^3 \quad (Z \gtrsim 136).$$

Similarly one obtains [32] the positron emission probability

$$\frac{dP_{e^+}}{dE_{e^+}} = h(E_{e^+}, Z_u) \exp\left[-\frac{2\hat{t}}{\hbar}(E_{e^+} + 2mc^2)\right].$$

Integration over positron kinetic energy E_{e^+} leads to the total emission probability.

$$P_{e^+} = i(Z_u) \exp\left(\frac{-4m_e c^2 \hat{t}}{\hbar}\right).$$

Exchanging $\hat{t}$ by the equivalent t_0 gives an analogous scaling behaviour as for δ-electron emission:

$$P_{e^+} \simeq i(Z_u) \exp(-2q_{\min} R_{\min}).$$

The scaling factors $h(E_{e^+}, Z_u)$ and $i(Z_u)$ contain the electronic densities and the nuclear Fermi function to describe positron repulsion from the Coulomb field. $q_{\min}$ defines the minimal momentum transfer given by

$$\hbar q_{\min} = \frac{|E_i + E_f|}{v_p} \simeq \frac{2m_e c^2}{v_p}$$

which is necessary to ionize the bound electron with energy E_i to a final state with the continuum energy E_f if the incident projectile velocity is v_p. Increasing $q_{\min}$ values (from larger binding energies) are responsible for a reduction of δ-electron emission and K-hole production probabilities for $Z_u > 170$ in spite of the ongoing increase of the electronic densities. For positrons, however, $q_{\min}$ decreases with increase of the binding energy of the innermost shells leading to a further enhancement of positron emission probabilities then mostly associated with a capture of the electron in empty bound states instead of direct ionization into the positive continuum. These formulae give insight into the QA transitions, but a quantitatively correct description of the transition probabilities is beyond the first order calculation and needs the full coupled channel approach.

The predicted exponential dependence of the excitation probabilities on the momentum transfer is characteristic for a Coulomb ionization mechanism [33]. Several approaches can be used to experimentally investigate QA's created in heavy-ion collisions: δ-electron emission, quasi-molecular X-ray (MO-X-ray) or characteristic X-ray emission from the separated atoms or emission of positrons. Here we mention a few selected examples.

a) *K-hole production:* A measurement of the K-hole production via the yield of characteristic X-ray emission in ^{208}Pb+^{208}Pb collisions furnishes the first experimental prove for the formation of QA's. The elegant experiment used the X-ray Doppler shift to correlate the X-ray yield with the $R_{\min}$ value of the collision. The steep increase at closest $R_{\min}$ is found in excellent agreement with the above described predictions. The $1s\sigma$ and $2p\sigma$ hole probabilities reach values of 20% and 80%, respectively, for closest collisions [34].
The scaling behaviour of K-hole production is demonstrated by plotting the reduced $1s\sigma$ excitation probability $P_{1s\sigma}/D\,(Z_u)$ versus $R_{\min}q_{\min}$ for a set of HI collision systems with $Z_u > 137$ [35] (Fig. 2). The full line, which represents the universal scaling law derived above, agrees well with the data. These results fully confirm the validity of the mechanism of the QA picture of HI collisions over a wide range of Z_u. However, first-order perturbation theory underestimates the measured data by factors of two to three in the absolute scale. Full agreement between measurement and theory is obtained using the complete coupled-channel calculations.

b) *δ-electron emission:* Explicit measurements of the double-differential δ-electron cross section have been performed both in inclusive measurements of electron spectra as well as for δ-rays in coincidence with subsequent K X-rays. The latter measurement in addition defines the initial state of the ejected electron. For light and asymmetric systems ($Z_u < 137$) electron production can be described in the framework

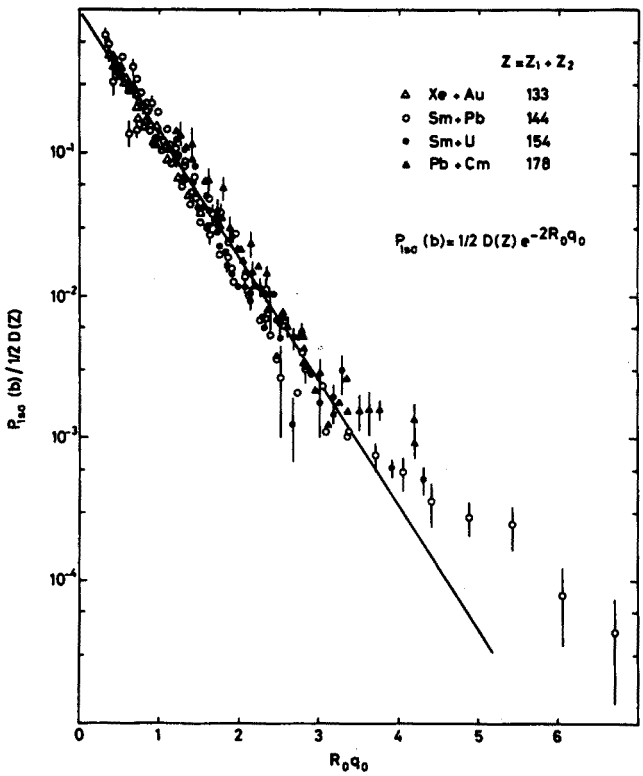

Fig. 2. Generalized excitation probability $P_{1s\sigma}/\frac{1}{2}D(Z)$ as a function of $R_{\min} \cdot q_{\min}$ for different collision systems (Reproduced from [35]).

of the Born approximation, where only electron emission due to the Coulomb field of the projectile is taken into account [36]. For heavier systems the full application of the QA picture is necessary for a reasonable description. Fig. 3 shows δ-electron cross sections for the Pb +Sn and Pb + Pb systems as function of the δ-electron kinetic energy. The actual presence of electrons with energies above 1 MeV is an exclusive feature of the QA mechanism; such energies exceed by about a factor of 20 the K-shell binding energy of a Pb-atom and by more than a factor of 100 the maximal energy that can be transferred to a free electron by heavy projectiles. The momentum transfer q, needed to result in such high energy electrons if formerly bound in a QA $1s\sigma$ state, by far exceeds the final electron momenta $\boldsymbol{k}_f$ on the order around 10 MeV/c^2.

Therefore, in order to fulfill momentum conservation, $\boldsymbol{k}_f = \boldsymbol{k}_i + \boldsymbol{q}$, the initial momentum $\boldsymbol{k}_i$ has to be comparable to the momentum transfer $\boldsymbol{q}$, *i.e.* on the order of 10 MeV/c^2 in this example. Such large intrinsic momenta can only be found in the strongly localized innermost QA electronic states.

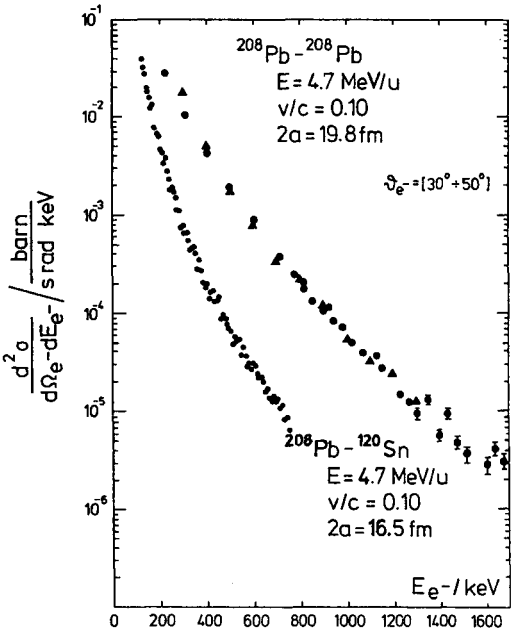

Fig. 3. The δ-ray spectra from Pb + Pb and Pb + Sn collision systems measured at the same relative velocity $v_\infty/c = 0.1$. Also indicated are the distances of closest approach for a head-on collision $2a$. Reproduced from [37].

The high-energy part of the δ-electron spectrum thus provides a direct information about the high-momentum components of the QA electron wave functions. The steeper fall-off of the Pb + Sn spectrum reflects the relative lack of high-momentum components for the bound state wave functions of this lighter system as compared to the Pb + Pb system with larger Z_u.

c) *positron production:* Atomic positron emission was first identified as an extra source in addition to the well-known nuclear IPC positron production in HI experiments at GSI in the late '70-ies by two independent experiments [38, 39]. Fig. 4 shows the experimental ratio of the excess of detected positrons over nuclear positron emission (IPC) (with the positron yield integrated over a positron kinetic energy range around 100 keV to 1 MeV) for different colliding systems with increasing Z_u. For constant $R_{\min}$ and projectile velocity v_p the excess yield increases as Z_u^{20} in excellent agreement with theoretical QA predictions. The continuing increase of positron production at large Z_u other than δ-electron emission proves the inclusion of strongly bound QA orbits in the positron production mechanism in addition to direct continuum–continuum transitions as mentioned above. Similar to the ionization probability of the innermost electrons, the QA positron

production probability was predicted to fall off rapidly (nearly exponentially) with increasing $R_{\min}$ as outlined above. This behaviour is presented in Fig. 5, where a comparison of the experimental and theoretical production probabilities are shown for three heavy collision systems as a function of $R_{\min}/2a$ [39]. Essentially comparable slopes for the three different collision systems clearly reflect the global validity of a Coulomb ionization mechanism for this positron source [33].

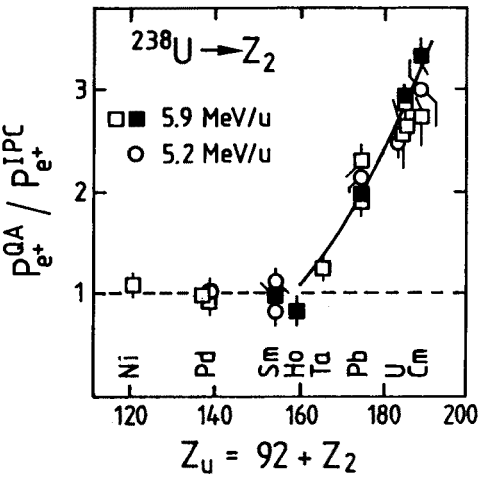

Fig. 4. The ratio of the positron production in HI collision to positrons from nuclear IPC processes as a function of Z_u. (Reproduced from [38]).

In summing, the actual formation of a QA in very heavy ion collision systems is experimentally well approved by the correct observation of the predicted ionization and emission processes characteristic for the transient formation of the QA. These findings formed the basis for an exciting search for the fundamental process of resonant positron emission — known as spontaneous positron production. It led to the detection of so far unexplained phenomena of monoenergetic positron emission and monoenergetic electron–positron pair emission. This research has mainly been performed by the EPOS and ORANGE collaborations at GSI. Important specific information to that field is elaborated by the TORI and the Z4 group in addition concentrating on the measurement of nuclear time delays by means of δ-electron and positron spectra [41, 42]. This article concentrates on discussion of the development of the EPOS experiments including the setup. For more general reviews of the positron experiments we refer to [43] and references therein.

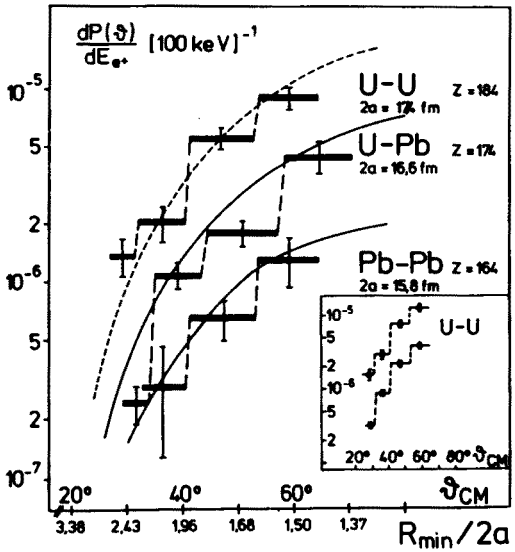

Fig. 5. Energy differential atomic positron production probabilities as a function of the laboratory scattering angle Θ_p. The solid lines represent the results of calculations [40]. The insert shows the total number of observed positrons per scattered particle. (Reproduced from [39]).

3. Concept of the EPOS solenoid positron- and pair-spectrometer

The experimental situation for the detection of leptons in HI collisions is obvious from Fig. 6, where typical yields of the competing positron, electron and γ-ray production processes for U + Th collisions at 5.85 MeV/u are shown. The production rates for positrons are smaller by factors of 10^4 to 10^5 than for δ-electrons or γ-rays [44]. In view of this, experiments for positron detection after HI collisions have to provide for:

- high positron detection efficiency throughout the full energy range of interest ($\sim$100 keV to $\sim$1 MeV) in order to cope with the small cross sections,
- reasonable energy resolution, in the order of 10 to 20 keV, significantly below the widths due to kinematic broadening in the laboratory system spectra, due to emission from fast moving systems,
- high selectivity for the detection of positrons to fully discriminate the copious background,
- reasonable lepton angular resolution; this feature became important throughout the later electron positron coincidence experiments,
- complete measurements of the HI collision parameters; this is to trigger quasi-elastic collisions and to determine $R_{\min}$-values defining the strength of the QA Coulomb potential,

- simultaneous γ-ray measurements at energies $E_\gamma > 2m_ec^2$; from these spectra the IPC yield of the nuclear transitions are derived.

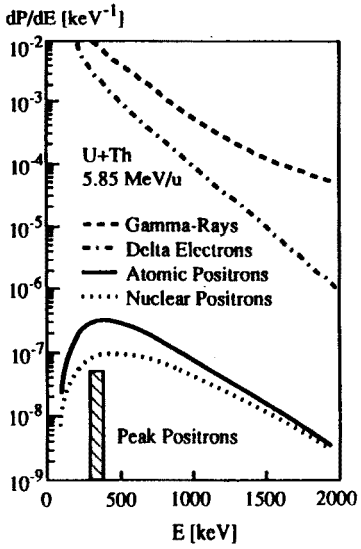

Fig. 6. The production probability of γ-rays, δ-electrons QA and nuclear positrons as indicated in coincidence with ions scattered into the angular region $25° \leq \theta_{HI} \leq 65°$ for the U + Th collisions at a beam energy of 5.85 MeV/u. The hatched area stands for the single positron lines. Reproduced from [18].

The EPOS spectrometer was designed to fulfill these demands [5–8]. A schematic view of the version of the setup being optimized for the coincident electron positron detection is shown in Fig. 7. We here give a brief description of the principle operation and its features.

Using a magnetic field, positrons and electrons are simultaneously transported off from the highly radioactive target region in either of the two arms of magnetic solenoid arranged perpendicular to the beam direction. The setup is optimized for effective and selective positron detection making use of principle features of solenoidal transport fields: any charged particle starting from the axis of the solenoid returns periodically to this axis. Thus, a detector placed along the solenoid axis is the natural choice for an effective detection geometry. A special Si(Li) solid state detector built as a slim pencil-like cylinder of 1 cm diameter and 10 cm length is just located on this axis in the right arm of the solenoid (at a distance of 83.2 cm from the target) for positron detection. Its small radial dimension represents an only small solid angle of about 1.2×10^{-4} sr for γ-rays or neutrons produced

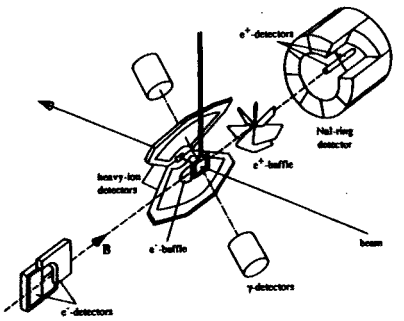

Fig. 7. A perspective view of the EPOS spectrometer in its configuration from 1988.

in the target which renders the background rates of these sources negligible. The high intensity of low-energetic δ-electrons is actively suppressed by means of a spiral baffle utilizing the opposite spiral directions of electron and positron trajectories in the magnetic field. Positrons are moreover identified by their characteristic 511 keV annihilation radiation being measured in the array of 8 NaI(Tl) crystals, which cylindrically surround the positron detector. The positron peak detection efficiency amounts to $\epsilon^{e^+}_{\mathbf{max}} = 14\%$ of 4π with $\epsilon^{e^+} > \epsilon^{e^+}_{\mathbf{max}}/2$ from 110 keV to 800 keV including the detection of at least one annihilation γ-ray in the NaI ring-detector. The Si(Li) detector energy resolution amounts typically to $\Delta E \approx 10$ keV.

For electron detection a pair of planar Si(Li) detectors is used. Again its geometry utilizes special features of electron paths in magnetic solenoid fields. The two detectors are mounted with their surfaces parallel to the solenoid axis but radially removed from the axis by a distance of 17 mm. This geometry avoids the detection of intense low-energy δ-electrons with $E \leq 120$ keV since these trajectories have too small radial sizes to reach the detectors. Low-energy electrons are moreover suppressed by the action of a small sheet baffle placed along the axis close to the target. The peak efficiency for detection of electrons amounts to $\epsilon_{\mathbf{max}} = 17\%$ of 4π with a width of the efficiency distribution covering the whole range of interest of

> 150 keV to ~ 1 MeV. Both electron and positron detectors are segmented to allow for some determination of the lepton emission angles (with respect to the beam axis) utilizing the correspondence between the emission direction and the detector hit position [19]. Moreover, the electron detectors need segmentation to cope with the high electron multiplicity.

Positrons and electrons are principally detected in coincidence with the scattered HI's in two Parallel Plate Avalanche Counters(PPAC) [45]. The measurement of HI scattering angles with respect to the beam axis ranges from $20° < \theta_{HI} < 70°$ and $-65° < \phi_{HI} < 65°$, where θ and ϕ are the polar and azimuthal ion scattering angles, respectively. These detectors fully determine the elastic HI kinematics with an ion angular resolution of $\Delta\theta \simeq 1.0°$. Any inelasticity or mass transfer can be limited from the ion angular measurement to ± 20 MeV or ± 5 amu, respectively.

The γ-radiation is monitored with two NaI(Tl) detectors placed at a direction inclined by 45° to the beam axis in the forward and backward hemispheres, respectively. The measured γ-ray energy distributions are transformed during the analysis into positron energy distributions via known IPC coefficients taking reasonable assumptions on the type and multipolarity of the transitions. These calculated positron spectra determine the nuclear IPC part of the measured positron yield [46, 44, 47].

We mention that the ORANGE and TORI groups have similar but in several aspects complementary approaches to measure positrons. In all experiments magnetic transport systems are used to detect positrons safely at places of low radioactivity. However, the suppression techniques for the intense flow of electrons are different. The ORANGE group uses two dispersive, large acceptance magnetic toroidal spectrometers (ORANGE-type β spectrometers) to detect separately positrons and electrons at extended special detectors placed at the focal areas of two spectrometers. This technique provides an extremely clean positron detection at highest luminosity but limits positron detection for backward and electron detection for forward emission according to the selected geometry and magnetic field settings. The TORI collaboration utilizes an S-shaped solenoid separating electrons and positrons magnetically by means of their opposite drift velocities in the curved magnetic field directed perpendicular to the solenoid plane [41].

4. Inclusive positron spectra

4.1. The line phenomenon

In Section 2 we discussed characteristic QA mechanisms and their experimental verification including induced QA positron emission. In addition to the continuous energy spectra from this source and of the IPC background,

the EPOS and the ORANGE collaboration identified peak-like structures in inclusive positron single spectra after HI-collisions in independent experiments [10, 12]. Studies performed by the EPOS group with collisions of uranium ions on curium targets at energies near the Coulomb barrier revealed a narrow peak at (316 ± 10 keV), exploiting a width of $\sim$ 70 keV [10].

Similar lines were later on observed at comparable kinetic energies around 300 to 400 keV in Th + Cm, U + U, Th + U, Th + Th and Th + Ta (EPOS) (Fig. 8) as well as in U + U, U + Pb and Pb + Pb (ORANGE). The lines were most clearly observed if particular broad but sharply defined ion angular regions were selected. These selections differ for the various lines and systems. The windows are essentially located well within the binary collision quasi-elastic regime allowing for an energy and mass transfer of less than 20 MeV and 5 amu, respectively, according the ion angular resolution. However, a correspondence of these favourable angular bins to other reaction channels cannot be excluded on the basis of a measurement of scattering angles only. The observed scattering angles are influenced from the ionic charge states which may considerably differ from the velocity dependent equilibrium values. An actual interconnection between non-equilibrium charge states and the production of the lines could thus well improve the peak-to-background ratio of the lines but this possibility has to be further investigated.

The widths of the positron lines are all similar and are essentially consistent with the assumption of a kinematic broadening due to the emission from the HI center-of-mass system. The cross sections of the lines can only be estimated because of the poor knowledge of the actual scattering process, assuming the lines are correlated with elastic scattering. The EPOS data reveal an essentially constant cross section of the order of 10 μb/sr over a range of $163 \leq Z_u \leq 188$, whereas the ORANGE data may not exclude a steep increase with Z_u^{18}.

The observation of narrow positron lines is an interesting phenomenon in itself, since the positron, being a particle of antimatter in our world, only appears transiently and, depending on the mechanism of its production, usually not monoenergetic. The well-known IPC or the newly found QA positron emission as well as nuclear β^+-decay typically all exploit continuous energy distributions as a matter of phase space. Monoenergetic positron emission implies a resonance phenomenon or a two-body elementary particle decay; both mechanisms limiting the phasespace. The finding of the lines in heaviest systems where the formation of QA's exclusively takes place suggested to try the process of spontaneous positron emission as an explanation. In fact, the search for this resonant QA process was the original motivation for these experiments. Trying such interpretation, however, implicitly includes that the QA lives for a long period on the order of $\sim 10^{-19}$ s as a

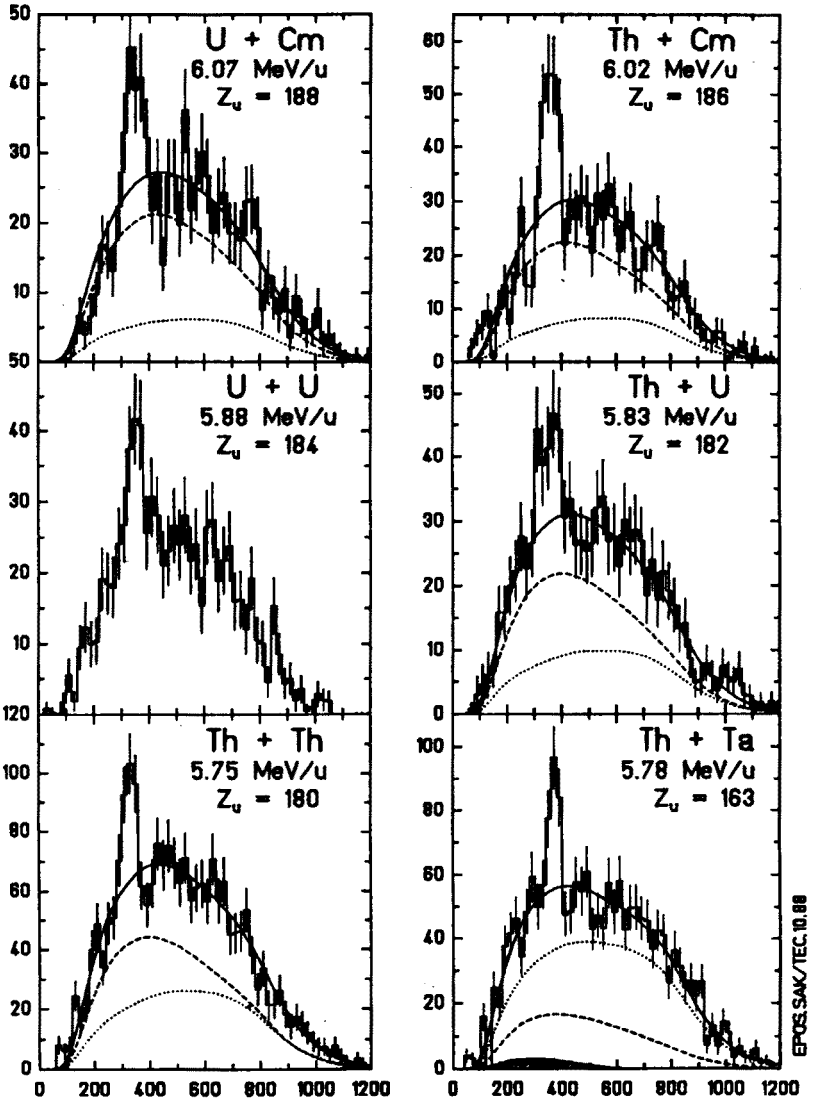

Fig. 8. The single positron lines family observed with the indicated HI-collision systems by the EPOS collaboration. The dashed and dotted lines present the positron contribution as expected from induced QA and nuclear processes, respectively. The solid line is the sum of both contributions [17].

consequence of the uncertainty relation, being long as compared to typical collision times of 10^{-21} s (see Fig. 1). It has been suggested that long-living ($\sim 10^{-19}$ s) heavy nuclear molecules may be formed transiently by attractive nuclear interaction as derived in a liquid drop model approach

[48]. The finding of an essential independence of the lines energies in the wide range of collision systems and the presence of lines even in subcritical ($Z_u < 173$) systems, where no spontaneous emission is expected, dismissed this exciting explanation. Contrary to the experimental observation the QA theory predicts a strong dependence of the spontaneous positron emission line-energies from Z_u in agreement with the variation of the overcritical binding energies. In Fig. 9 the predicted energies are compared with the experimentally observed energies for various assumptions for the di-nuclear shapes and the ionic charge of the QA's. The assumption of a completely spherical nuclear formation, with the aim to better match the data, seems to be unrealistic. Moreover, the high resolution measurements of the ORANGE collaboration showed, that more than one line can be observed in the measured positron energy distributions of one collision system [9, 49].

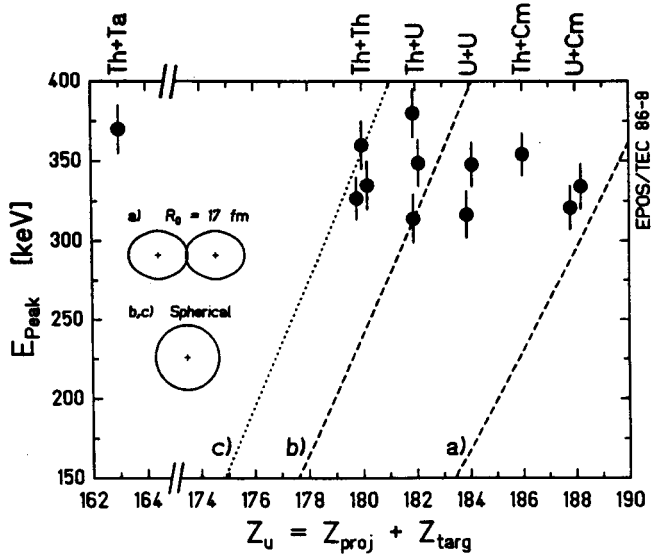

Fig. 9. Mean energies of the positron peaks as a function of Z_u. The lines present calculations for spontaneous positron emission assuming the formation of different (long-living) di-nuclear systems:(a) a complex with internuclear separations fixed at $R \approx 17$ f, (b) and (c) spherical configuration. Electron screening is included in (a) and (b), but a fully stripped compound system is assumed in (c).

What could be the source of these lines? Before speculating about possible exotic explanations, all conventional scenarios first have to be carefully investigated. The most obvious process leading to positron emission is nuclear IPC of nuclear transitions emission although generally of continuous positron energy distributions. An examination of the simultaneously measured γ-ray spectra provides a direct test for this suspicion. Assuming

E1 (or other higher multipolarities and type of transitions) the necessary strength of the γ-ray branch can be calculated from known IPC coefficients. Higher multipolarities than E1 give less strength in the γ-ray spectra. E0 transitions escape from this test and need the inspection of internal conversion electron (IC) spectra. IPC proceeds through the emission of electron positron pairs with the energy of the leptons distributed up to the maximally available energy of $E_{\max} = E_\gamma - 2m_e c^2$. For heavy systems the Coulomb potential desymmetrizes the lepton spectra significantly with a preference for high-energy positrons and low-energy electrons. This effect reduces the width of the positron energy distribution as compared to the low $-Z$ case and shifts the centroid nearer to $E_{\max}$. But even a favourable choice of $E_{\max}$ results in widths of not less than $\sim$ 150 keV which still considerably exceeds the observed 80 keV of the lines. Neglecting this inconsistency, an inspection of the measured γ-ray spectrum is shown in Fig. 10 (a). The comparison is made for an expected γ-ray line with a yield as expected from the positron line intensity. It correctly includes Doppler broadening according the HI kinematics and energy resolutions.

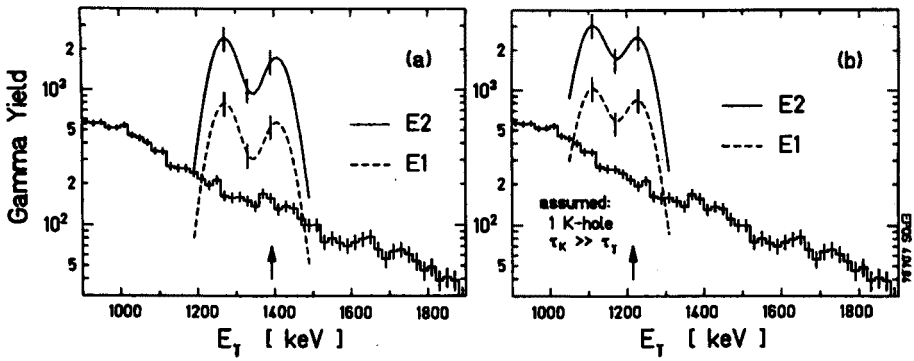

Fig. 10. Pair conversion calculated for γ-rays. The γ-ray yield is ploted as a function of the γ-ray energy E_γ for U + Cm collision system at a bombarding energy of 6.05 MeV/u. The γ-ray structure (calculated by [18]) is shown which would accompany the positron peak in the case of E1 or E2 nuclear transition in uranium, assuming the positron peak is caused by IPC in part (a) or MIPC in part (b).

A rare variant of IPC is monoenergetic IPC (MIPC). This occurs, if the electron of the IPC pair is captured in an empty atomic shell, most probable the K-shell, resulting in a reduction of the phase space and thus the emission of a positron of fixed energy. This process is more adequate to the narrow positron lines but sensitively depends on the K-shell hole probability. Even

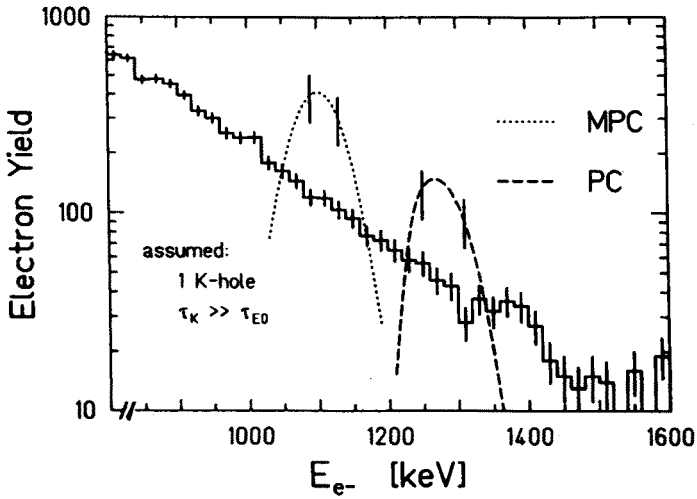

Fig. 11. Pair conversion calculated for electrons. The electron yield is plotted as a function of the electron kinetic energy for the U + Cm collision system at a bombarding energy of 6.05 MeV/u [18]. The electron structure associated with the positron peak is shown for IPC and MIPC assuming the positron peak is caused by E0 nuclear transition in uranium.

assuming the very improbable case, that the lifetime of the 1s-hole is comparable to the nuclear transition, the respective comparison with the measured γ-ray spectrum (Fig. 10 (b)) rules out also this scenario. An inspection of conversion electron spectra is shown in Fig. 11 for both IPC and MIPC now assuming an E0 multipolarity. To obtain this spectrum, electrons were measured simultaneously in the EPOS set-up with their emission angles restricted thus limiting kinematic broadening. Again no indication can be found in these spectra for a singular nuclear transition of sufficient strength. One yet very improbable scenario remains: MIPC occurring at an ion with both K-shells totally empty such that no IC can be observed. This seems to be very improbable in view of the usual 10^{-16} s lifetimes for K-holes. It is moreover difficult to further assume, that no IC takes place from any other shell and, not to forget, MIPC has to be necessarily accompanied by the stronger continuous IPC-branch, but no indication for IPC distribution has been observed in the positron spectra at higher respective energies. In this completeness these investigations have only been made for the U + Cm system. But for all ion-atom combinations investigated the simultaneously measured NaI-γ-ray spectra have always been carefully inspected for strong singular nuclear transitions but with negative results [10, 12, 18].

4.2. Background determination

Quoting reliable values for the production probabilities of the positron lines depends crucially on a quantitative evaluation of the trivial part of the spectrum. This part originates from two main sources: IPC of closely lying transitions in the highly excited nuclei and induced QA positron emission. In principle, the cross sections of these two mechanisms are well accessible. The IPC rate is determined from the yield of nuclear transitions with energies exceeding $2m_ec^2$ which — except E0-transitions — can be derived from the γ-ray spectra measured simultaneously in the experiment. The yield of the QA production is taken from the theory. In practice, however, the straight-forward computation of the IPC rate suffers from the insufficient knowledge of the electromagnetic character and multipolarity of the nuclear transitions and for the QA cross section from uncertainties in the primary degree of ionization of the ions. Therefore a consistent description of the experimental yield of both contributions was developed [47] on the basis of the total set of γ-ray and positron spectra from all collision systems measured ($163 < Z_{ua} < 188$). IPC dominates the positron background of the low-Z systems and the QA production the high-Z combinations.

The analysis [50] follows a decomposition of the positron production probability per heavy-ion collision into an incoherent sum of the two obvious contributions:

$$\frac{dP}{dE_{e^+}} = \sum_{ij} \int_{2m_0c^2}^{\infty} \frac{d\beta_i}{dE_{e^+}}(E_\gamma, Z_j) \frac{dP^N}{dE_\gamma}(b, Z, E_1) dE_\gamma + f^{QA}(Z_u, b, E_1) \frac{dP^{QA}}{dE_{e^+}}(Z_u, b, E_1) .$$

The first part, representing the nuclear contribution, originates in the rest frame of nucleus j, being either the target- or the projectile-like scattered nucleus. It is a function of the nucleus j, the projectile energy E_1 and the Coulomb strength proportional to $Z = Z_1 Z_2$. The IPC coefficient β_i, here expressed in its differential form, depends on the nuclear transition energy E_γ, the nuclear charge Z_j and on the electromagnetic transition type and multipolarity indicated by index i [51, 52]. For the present analysis we consider only multipolarities E1 and E2 which are known to dominate in this energy regime [53]. Throughout the fit procedure the nuclear γ-ray spectrum $dP_N/dE_\gamma(b, Z, E_1)$ is analytically described by spectral shape functions $f_i(E_\gamma, b, E_1)$ of E1 and E2 components. The E1-transitions, with their origin in the statistical regime of nuclear states, are characterized by nearly exponentially declining shapes, in accordance with the statistical

nature of the transitions. The E2-shape function is characterized by a bump around $E_\gamma \simeq 1.2$ MeV with the high-energetic slope declining exponentially as well. The spectral functions f_i are related to the energy-dependent E1/E2 mixing amplitudes

$$F_i(E_\gamma, b, E_1) = \frac{f_i(E_\gamma, b, E_1)}{\sum_i f_i(E_\gamma, b, E_1)}.$$

The second part standing for the QA production is described by the differential QA positron emission probability given in the HI CM rest frame. The QA theory [40] is uncertain by a scaling factor f^{QA}, considering the degree of ionization in the incoming channel usually approximated by introducing a Fermi level above the $d_{3/2}$ QA states.

The result of the background calculations is presented in Fig. 8. The calculated positron spectra are corrected for efficiency and line shape of the positron detector and are transformed into the LS. Dashed and dotted lines indicate the positron contributions from the QA and nuclear processes, respectively. The solid lines is the sum of both contributions which, besides the peak structures, excellently describe the measured data. The increase of the QA positron contributions with Z_u is obvious from the area under the dashed lines, starting with a $\approx 20\%$ share for $Z_u = 163$ to a $\approx 80\%$ for $Z_u = 188$. This description of the background is characterized by a global energy-dependent E1/E2 multipolarity mixing and a global QA scaling factor of $f^{QA} = 1.00 \pm 0.08$. It is obtained for the global spectra integrated over the experimental range of impact parameters and for a close range of beam energies around the Coulomb-barrier. Increasing the impact energy or selecting closest collisions will enhance the E1 part over E2, thereby leading to larger IPC contributions in the positron spectra. The overshoot of the remaining experimental positron yield after subtracting the IPC part (Fig. 12) observed for increased beam energies in U+Ta is an indication for this tendency. However, the present data have not sufficient statistical quality to derive the impact parameter and beam energy dependances of the peak quantitatively.

With these uncertainties in mind we estimate the accuracy of the present background computation to within $\pm 20\%$. This bound of the continuous background allows to determine reliably the intensity of the positron peaks. Giving the yields in terms of production probabilities per collision or in cross sections, however, needs a further comment. The quoted values assume elastic scattering ignoring any mass or energy transfer. However, the obvious dependence of the peak-to-background ratio on the selection of particular ion angular ranges neighbouring the pure elastic domain could indicate that inelastic reaction channels are involved. We estimate that the given cross sections are uncertain by a factor of 2 in addition to the quoted purely statistical error. This can be more uncertain if the assumption of an isotropic

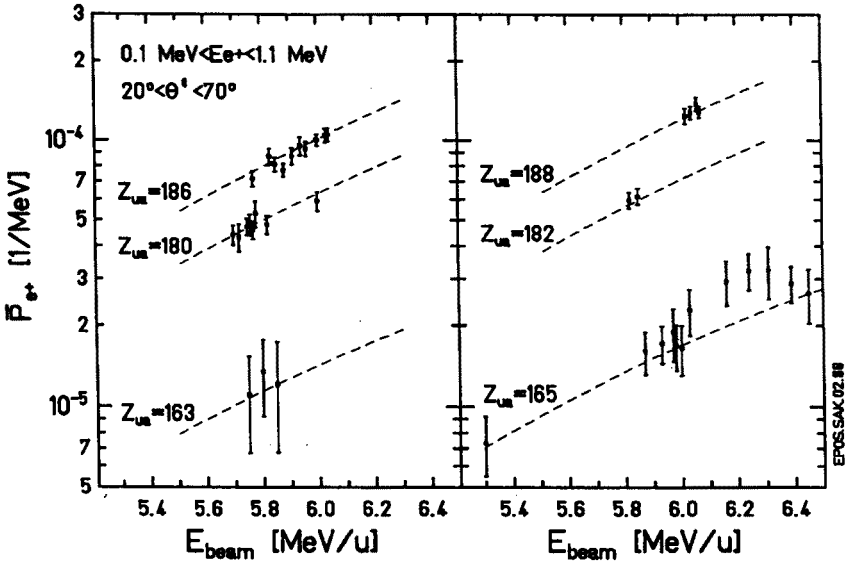

Fig. 12. Energy dependence of the positron production as a function of projectile energy for different projectile-target systems (integrated in the region 0.1 MeV $\leq E_{e+} \leq$ 1.0 MeV and $20° \leq \theta \leq 70°$).

positron emission both for the IPC and QA channel can not be made. The anomalous lines found so far are observed with essentially constant cross-sections around 10 μb/sr. For example, the 316 keV U+Cm line [10] exploits a probability per elastically scattered HI event of $P_{e+} = (2.5 \pm 0.5) \times 10^{-5}$ corresponding to a cross-section of $d\sigma_{e+}/d\Omega_{\mathrm{HI}} \cong 12.9 \pm 2.5$ μb/sr. No pronounced systematic variation of the cross-section value over the large experimental range of Z_u from 163 to 188 was found. An experimental limit on the decrease of σ_{e+} over this range lies within a factor of 2 to 3 for the EPOS data. In terms of a power law dependence of the cross-section on Z_u, $\sigma_{e+} \propto Z_u^n$, the data places an upper limit of the exponent factor at $n \leq 8$. Any production mechanism which implies a larger exponent of the spontaneous positron emission process with around 20 thus appears very unlikely to explain the total set of the lines (although for individual lines like the 316 keV U+Cm line such origin cannot be dismissed from these systematics). We mention, that the ORANGE group reports a Z_u^{18} dependence from their data. Here, further investigations are needed also to investigate the influence of a trivial dependence like an eventual beam energy dependence on the line production cross section.

5. Positron-electron coincidence measurements

The lines in the inclusive positron spectra [10] were found for various heavy systems at essentially equal energies. Known conventional mechanisms, including QA spontaneous positron emission failed to explain the lines consistently. There the speculative possibility was raised, that the source of the phenomenon could be the two-body decay of a previously undetected neutral system. Although the finding of even narrower lines in the energy sum spectrum of coincidently emitted electrons and positrons, the original idea of a fundamental particle like the axion [54, 22, 23] was soon totally disproved. Nevertheless a composite system as the natural alternative if a point-like source is excluded, can still not be completely dismissed. Thus it appears worthwhile to pass through the experimental facts found for the phenomenon of narrow electron positron line emission within the subsequent investigations with the EPOS spectrometer.

Within the above scenario the single positron lines energies imply an invariant mass around 1.8 MeV/c^2. The fiducial volume of the EPOS setup limits the lifetime of the source to some 10^{-10} s assuming that the object decays at high velocities as given by the kinematic HI velocities. Since the single positron lines widths were consistent with emission from the HI CM system, it appears most suggestive, that the source for the related two-body decay into an e^+e^- pair is at least approximately, at rest in the HI CM system. The typical back-to-back emission characteristic with $E_{e+} \sim E_{e-}$ then leads to a mutual cancellation of the individual Doppler shifts of the two leptons of the pair in the LS. This emission scenario offers the characteristic signature of a narrow line in the e^+e^- energy sum spectrum of the pairs at a position defined by the invariant mass of the decaying object (after subtracting the rest mass of the leptons). In order to efficiently observe this signature forward and backward lepton emission directions with respect to the beam velocity have to be measured simultaneously with equal efficiencies. This is ideally fulfilled in the EPOS setup with the solenoid mounted perpendicular to the beam direction. To match the single line cross sections it is sufficient, that the narrow sum line collects a small amount of only some percent of the total electron positron yield produced in HI collisions.

The goal of the subsequent electron positron coincidence experiments clearly was to test this exciting hypothesis. We shortly summarize how the EPOS setup results on the characteristic signature [18, 20]:

- Two complementary projections of the E_{e+} E_{e-} energy distribution are most helpful. a) Projection onto the energy sum $E_\Sigma = E_{e+} + E_{e-}$. There the width of the narrow line is mainly determined by the detector resolution of $\delta E_\Sigma \sim 15$ keV. b) Projection onto the difference energy

$E_\Delta = E_{e^+} - E_{e^-}$. There a broad line centered around zero is expected with a FWHM of $\delta E_\Delta \sim 120$ keV. The width δE_Δ is proportional to E_Σ and reflects the full kinematic broadening. The width δE_Δ is considerable narrower than the with expected for a background process like IPC covering the full phase space of a three-body decay. Hence the structure in the difference projection provides a good selection criterion for this scenario.

- A rough information on the angular correlation between the electron and positron of the pair is contained in the time-of-flight correlation (t_{e^+} vs t_{e^-}). Due to different e^+, e^- angular acceptance, the pattern is different for a back-to-back or a less correlated angular correlations like that of uncorrelated background pair emission. The differences in the time-of-flight pattern are based on the dependence of the transport time t on the lepton emission angles $\vartheta_\circ$ with respect to the solenoid axis with $t \propto 1/\cos\vartheta_0$ in uniform magnetic fields *i.e.* leptons emitted steeply to the axis arrive later than those emitted in the direction of the axis. The experimental time resolutions of the EPOS detectors are sufficient to divide the lepton angular ranges into two major parts, corresponding to steep (slow) and flat (fast) emission with respect to the solenoid axis. A detailed MC-study of the transport reveals that events from back-to-back emission processes are predominantly grouped in a fast-fast TOF window whereas the uncorrelated background pair emission results in an essentially uniform TOF distribution. The uncorrelated background can thus be reduced by factors around six with no essential loss for the back-to-back pair events.

Electron positron coincidence experiments have been performed in the EPOS setup with ^{238}U + ^{232}Th (5.80 – 5.90 MeV/u) and ^{238}U + ^{181}Ta (5.8 – 6.7 MeV/u) collision systems [18–20]. Fig. 13 shows the resulting electron positron sum-energy spectra together with the associated difference energy distributions. The difference energy spectra are restricted to the events contained within a window closely around the respective sum energy line. The striking features of the data are the very narrow prominent sum-energy lines. The lines widths are only slightly larger than what corresponds to the instrumental resolution and, in particular, are much narrower than the respective broad structures in the difference-energy distributions. This pattern indicates a mutual cancellation of the original Doppler. For comparison, broadened lines with widths $\simeq$ 140 keV are expected in the sum energy spectrum for emission from either of the fast moving scattered ions ($v > 0.04c$) or from the HI CM ($v \approx 0.05c$) if the leptons of the pair are totally uncorrelated.

Within statistical uncertainty the lines group around mean sum energies of $\sim$ 620 keV, $\sim$ 750 keV and $\sim$ 810 keV (see Table I). Taking the sum-lines

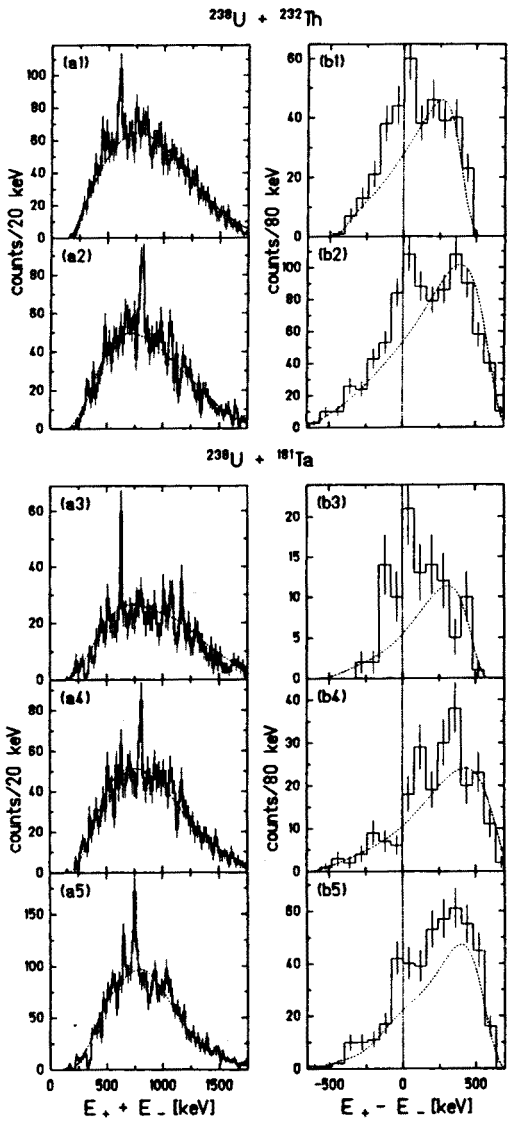

Fig. 13. Sum-energy spectra measured with the EPOS spectrometer for U + Th and U + Ta collisions. The spectra are gated by different $e^{\pm}$ time-of-flight windows, but no conditions on the heavy-ion scattering (except the global restriction on quasi-elastic scattering) have been imposed. Reproduced from [20].

as the signature for a two body decay from an object approximately at rest in the HI CM system, this grouping implies the existence of different intrinsic states or configurations of such objects. This experimental circumstance

TABLE I

Summary of results from EPOS and ORANGE experiments. Results presented at PANIC XII Conference (June 25–29, 1990) by P. Salabura and W. Koenig, and published in [61].

System	U+Ta	U+Ta	U+Pb	U+Th	U+U
Group	EPOS	ORANGE	ORANGE	EPOS	ORANGE
E_{beam} (MeV/u)	5.3–6.8	6.3	5.9	5.8–5.9	5.8–6.0
ρ_{target} (μ/gcm^2)	600	1000	850[a]	300[a,b]	400[a]
			Line 1 ~ 560 keV		
E_{beam}	5.3–6.8		5.9		5.8
E_Σ (keV)		[c]	547±6	[c]	554±6
$\langle E_\Delta \rangle$ (keV)			~ 0[e]		~ +15[e]
$\vartheta_{e^+e^-}$			180°±18°		(70°–150°)[d]
			Line 2 ~ 620 keV		
E_{beam}	6.24–6.38	6.3	5.9	5.85–5.9	5.8
E_Σ (keV)	625±8	635±6		608±8	635±6
$\langle E_\Delta \rangle$ (keV)	+30	+90[e]		~ 0	+10
$\vartheta_{e^+e^-}$	(90°–180°)[d]	(90°–180°)[d]		(70°–150°)[d]	(70°–150°)[d]
			Line 3 ~ 755 keV		
E_{beam}	5.93–6.76	6.3	5.9	5.83	5.8–6.0
E_Σ (keV)	748±8			760±20 (weak)	
$\langle E_\Delta \rangle$ (keV)	~ 150			~ 0	
$\vartheta_{e^+e^-}$	(60°–120°)			not measured	
			Line 4 ~ 805 keV		
E_{beam}	6.24–6.38	6.3	5.9	5.87	5.9
E_Σ (keV)	805±8	805±8	787±7	809±8	815±8
$\langle E_\Delta \rangle$ (keV)	+220	not analyzed	~ +10	~ +30	~ 0
$\vartheta_{e^+e^-}$	180°±30°	(90°–180°)[f]	180°±18°	180°±40°	~ 180°

[a] Sandwiched between 20/40μg/cm carbon

[b] ThF_4

[c] Reduced efficiency due to low energy cutoff

[d] Predominantly in this angular range

[e] Corrected for mean Doppler shift of (30–40) keV, assuming that mean emitter velocity $\approx$ c.m. velocity. In cases of U+Pb and U+U limited range of observation, FWHM ~ 150 keV

[f] preliminary

is difficult to accomplish by a fundamental object, except one accepts the existence of a whole family of unknown particles. But any fundamental and/or point like objects have meanwhile completely been dismissed as the source of the lines by independent measurements mainly resonant Bhabha scattering (RESBHA) [55–58] or beam dump experiments [59]. Composed objects with sizes of the order of the electron Compton wave length, which quite naturally could explain the diversity of line energies, are still not explicitly excluded.

Other observations connected with the lines however disagree with the above two-body decay scenario. Only the 810 keV line group essentially exhibit an electron positron TOF correlation as expected for back-to-back emission in the EPOS system, the other line groups around 620 and 750 keV are in conflict with this pattern. From Table I and Fig. 13 it is also apparent, that while the U + Th lines exhibit difference -energy distributions essentially centered around $E_\Delta = 0$ keV, the difference energies are wider and systematically shifted to higher positron and lower electron energies for the U + Ta collisions. These energy shifts have the correct sign for a final state interaction of the leptons with the Coulomb field of the heavy ions.

A measurement of the electron positron opening angle distribution could finally decide on the validity of the two-body decay scenario. However, this is a major difficulty, because at the given low lepton energies angular straggling by multiple scattering in the target partly destroys this information (*e.g.* a $\sim 300\mu$gcm target causes, besides energy loss, an angular straggling of $\sim 10°$). At the same time this precludes the application of tracking techniques conventionally used for the invariant mass measurements in high energy physics. The solenoid-specific time-of-flight technique applied here as described above is an indirect method to derive the angular distribution within these physical limits. The results also taking into account the still poor statistics are given in Table I.

A global but more direct measurement of the electron positron opening angle characteristic can be performed in EPOS by the position sensitive Si(Li) detectors. This method utilizes the correspondence between the lepton azimuthal emission angle (around the solenoid axis) and the place of incidence on the detector. It has first been applied for U + Ta collisions [20]. For the $\sim$ 620 keV and $\sim$ 810 keV lines the result confirmed the angular correlations deduced from the TOF. The line at $\sim$ 748 keV observed most prominent in this system was found to be preferentially associated with pairs forming smaller opening angles. The calculation of the background yield in the sum energy spectra (dashed lines in Fig. 13) based on the QA theory and the IPC yield similarly as it was derived for the inclusive positron single spectra. An additional yield of IC electrons is taken into account by adjusting the experimentally measured electron multiplicity. This

background calculation is assumed to be accurate within $\sim 20\%$. The calculation is made by MC-techniques with the MC-events passing through the identical analysis procedure as the original data. The good knowledge of the smooth part allows to study the yield of the peak events. A first but rough study of the yield of the 748 keV (U + Ta) peak events as a function of $R_{\min}$ was limited by still poor statistics [47, 50]. An exponential increase with decreasing $R_{\min}$ according $\exp(-2\alpha R_{\min})$ with the slope constant $2\alpha = (0.35 \pm 0.07)\,\mathrm{fm}^{-1}$ characterizes the data up to nuclear distances close to the nuclear contact point. The other two sum-energy lines of this system indicate a similar behaviour but with even less statistics. Such exponential behavior compares with the dependencies of one-neutron transfer ($2\alpha = 1.08\,\mathrm{fm}^{-1}$ [60]) and QA positron production ($2\alpha = 0.13\,\mathrm{fm}^{-1}$). For the more symmetric U + Th system $R_{\min}$ cannot be resolved from the scattering angle distribution, although, also there the line events were found in quasielastic ion scattering regions. A first excitation function measurement was performed for the 748 keV U + Ta line, revealing a resonance-like behaviour around 6 MeV/u. This is kinematically consistent with the above described $R_{\min}$-behaviour assuming Rutherford (Coulomb) scattering.

A numerical comparison of the results of the EPOS and ORANGE experiments on the sum energy lines is given in Table I. The ORANGE group reports on sum-energy lines around ~ 550 keV, ~ 630 keV and ~ 805 keV. For the two lines around ~ 630 keV and ~ 805 keV, in the system U + Ta measured by both groups the experiments reveal similar observations: the ~ 805 keV line seems to be consistent with a back-to-back scenario, whereas the data from the ~ 630 keV structure reflect a more complicated angular dependence. For the 748 keV line with a strongly asymmetric share of the lepton energies, the ORANGE experiment needs a respectively asymmetric setting of the spectrometers currents not persuade at that time. The 630 keV U + Ta line of the ORANGE experiments was moreover strongest observed in coincidence with U-fission events. This reaction branch was not accessed in the EPOS experiments.

6. Future experiments

The second generation of the positron experiments at GSI culminated in the discovery of sharp electron-positron sum-energy lines as described in the previous chapter. This line phenomenon appears to be well established from the experiments by the two groups. The EPOS and ORANGE instruments offer considerably different approaches which, in some aspects, are complementary. Except from the cross sections, the two groups report similar observations on the global line characteristics [43]. The cross sections which were found to be of the order of 0.1 to 5 μb/sr, are difficult to determine. This is because of the poor knowledge on the lepton opening angle

correlations, the excitation function and on the reaction path. The $\sim$ 630 keV line has been found most prominent in deep inelastic collisions by the ORANGE group whereas all other lines were associated with quasielastic collisions.

A conceivable explanation for the source of the lines is totally missing until now. In this situation more systematic investigations of the production mechanism and the lepton emission characteristics at a level of better statistical evidence and improved experimental resolution are urgently needed. It is clear that a detailed study of the line properties involves many parameters and requires many-dimensional cuts in the experimental data, which drastically reduce the statistics. A new generation of experiments thus needs much higher data accumulation rates, in particular for electron positron-coincidence events. This involves raising the detection efficiencies of the instruments, developing instrumental strategies to allow for higher electron-counting rates and, last but not least, improving the ion-beam performance towards better beam-on beam-off ratios (ideally aiming a 100% duty cycle) to raise luminosities without increasing the random coincidence rates.

The recently installed EPOS II spectrometer [62] addresses the present experimental demands. The technique involved for measuring lepton angles is more precise: the instrumental distinction between forward and backward emission in the new setup is made energy independent and less sensitive to off-axis emission and is less distorted by lepton-backscattering in the detectors. Particular attention has been put to keep the whole transport volume clear of any material (except the necessary target and the detectors themselves), thus minimizing secondary processes like backscattering. Bremsstrahlung, external pair conversion *etc.*, which were partly suspected to result in the production of lines. In particular, no baffles have been used to mechanically block the electrons from reaching the positron-detectors or to suppress the huge low-energy δ-electron flux now achieved by other techniques.

The new apparatus (see Fig. 14) has been optimized for a most effective electron-positron pair detection in coincidence with the scattered heavy ions. Again this instrument is based on a magnetic solenoid for transport which is arranged perpendicular on both sides of the beam. Electrons and positrons are now simultaneously detected in both arms. Positron identification is made in two steps, first by utilizing the opposite spiral sense of the trajectories of positrons and electrons and second by detecting at least one annihilation γ-ray. This implies a newly designed concept of sandwich-like back-to-back arranged planer Si(Li)-detector arrays. Always a pair of these is mounted within the field parallel to the field lines on both ends of the solenoid but with a certain distance from the solenoid axis. The radial offset

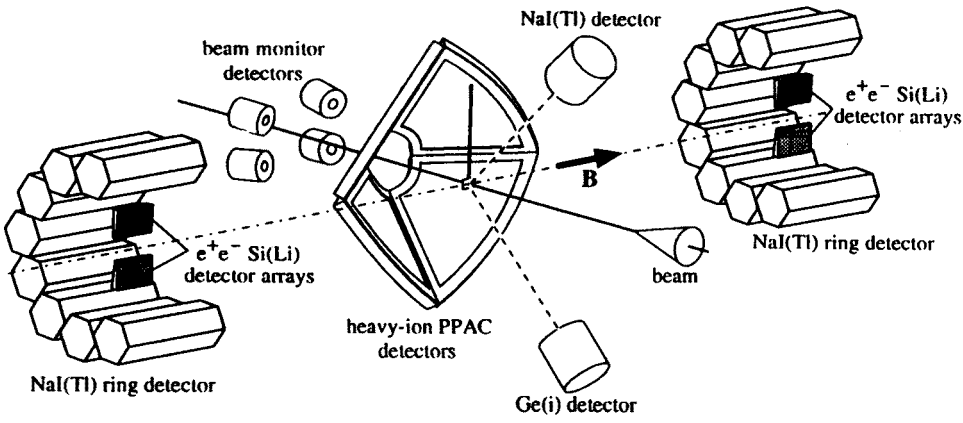

Fig. 14. A perspective view of the new EPOS spectrometer. The set-up shown is immersed in an uniform magnetic field $\boldsymbol{B}$, produced by 18 pancake coils (not shown in the picture). The field is oriented along the solenoid axis and is penpendicular to the beam.

from the axis is to cope with the flux of low-energy δ-electrons limited to cylinders of small spiral diameters around the solenoid axis. Left and right handed spiral trajectories associated with positrons and electrons, respectively, are identified by observing the signal in either of the two sides of the sandwich. In order to account for the high electron rates the Si(Li) detector wavers are segmented into six segments each. A redesign of the HI gas detectors improves the kinematic resolution and the accepted solid angle. The total gain in the electron positron-detection efficiency thus reaches up to a factor of 8 depending on the lepton opening angular distribution of the pair.

Besides the EPOS spectrometer also the ORANGE setup has been considerably upgraded for higher efficiencies and improved lepton angular resolution and moreover gains from a shorter micro-structure pulse distance in the duty cycle of the accelerator. The latter improvement is due to the installation of a new injector system based on an ECR-source, a RFQ and a IH-structure section. The hunt for the positron lines has also been started at a different laboratory. A new large solenoidal spectrometer APEX (**A**TLAS **P**ositron **EX**periment) [63] has reached its final assembly phase at the Argonne superconducting linear accelerator ATLAS. A combined effort of these three experiments will hopefully bring the answer to the "GSI electron positron puzzle" within the coming years.

REFERENCES

[1] W. Greiner, ed., *Quantum Electrodynamics of Strong Fields*, Plenum Press, N.Y. 1983.

[2] W. Greiner, B. Müller, J. Rafelski, *Quantum Electrodynamics of Strong Fields*, Springer Verlag, Berlin Heidelberg 1985.

[3] B. Müller, J. Rafelski, W. Griner, *Z. Phys.* **257**, 62 (1972).

[4] Ya.B. Zel'dowich, V.S. Popov, *Sov. Phys. Usp.* **14**, 673 (1972).

[5] A. Bałanda, H. Bokemeyer, H. Folger, S. Matsuki, D. Schwalm, P. Vincent, K. Bethge, A. Gruppe, W. Kessel, R. Schule, M. Waldschmidt, J.S. Greenberg, *GSI-proposal 175*, (1979).

[6] H. Bokemeyer, in *Selected Topics in Nuclear Structure*, ed. Z. Stachura, Uniwersytet Jagielloński, Kraków 1984, p. 335.

[7] H. Bokemeyer *et al.*, in *Physics of Strong Fields*, NATO ASI Series B: Physics Vol 153, ed. W. Greiner, Plenum Press, New York 1987.

[8] H. Bokemeyer, Report GSI-90-11.

[9] W. Koenig, F. Bosch, P. Kienle, C. Kozhuharov, H. Tsertos, E. Berdermann, S. Huchler and W. Wagner, *Z. Physik* **A328**, 235 (1987).

[10] J. Schweppe, A. Gruppe, K. Bethge, H. Bokemeyer, T.E. Cowan, H. Folger, J.S. Greenberg, H. Grein, S. Ito, R. Schule, D. Schwalm, K.E. Stiebing, N. Trautmann, P. Vincent, M. Waldschmidt, *Phys. Rev. Lett.* **51**, 2261 (1983).

[11] T.E. Cowan, H. Backe, M. Bergmann, K. Bethge, H. Bokemeyer, H. Folger, J.S. Greenberg,H. Grein, A. Gruppe, Y. Kido, M. Klüver, D. Schwalm, J. Schweppe, K.E. Stiebing, N. Trautmann, P. Vincent *Phys. Rev. Lett.* **54**, 1761 (1985).

[12] M. Clemente, E. Berdermann, P. Kienle, H. Tsertos, W. Wagner, C. Kozhuharov, F. Bosch and W. Koenig, *Phys. Lett.* **137B**, 41 (1984).

[13] H. Tsertos, E. Berdermann, F. Bosch, M. Clemente, P. Kienle, W. Koenig, C. Kozhuharov and W. Wagner, *Phys. Lett.* **162B**, 273 (1985).

[14] J.S. Greenberg, the first public mention of a possible new paricle as the explanation for the e^+-peaks, Nashville, October 1984.

[15] A. Schäfer, J. Reinhard, W. Greiner, B. Müller, G. Soff, *J. Phys. G* **11**, 69 (1985).

[16] A.B. Balantekin, C. Bottcher, M.R. Strayer, S.J. Lee, *Phys. Rev. Lett.* **55**, 461 (1985).

[17] T.E. Cowan, H. Backe, K. Bethge, H. Bokemeyer, H. Folger, J.S. Greenberg, K. Sakaguchi, D. Schwalm, J. Schweppe, K.E. Stiebing, P. Vincent *Phys. Rev. Lett.* **56**, 444 (1986).

[18] T.E. Cowan, Ph.D. Thesis, Yale University (1988).

[19] P. Salabura, Ph.D. Thesis, Jagiellonian University (1989), and GSI-report-90-06 (1990).

[20] P. Salabura, H. Backe, K. Bethge, H. Bokemeyer, T.E. Cowan, H. Folger, J.S. Greenberg, K. Sakaguchi, D. Schwalm, J. Schweppe, K.E. Stiebing, *Phys. Lett.* **B245**, 153 (1990).

[21] E. Berdermann, F. Bosch, P. Kienle, W. Koenig, C. Kozhuharov, S. Schuhbeck, H. Tsertos, S. Huchler, J. Kemmer, A. Schröter, *Nucl. Phys.* **A488**, 683c (1988).
[22] T.W. Donnelly *et al.*, *Phys. Rev.* **D18**, 1607 (1978).
[23] W.A. Bardeen, R.D. Peccei, T. Yanagida, *Nucl. Phys.* **B279**, 401 (1987).
[24] F.W.N. De Boer, K. Abrahams, A. Bałanda, H. Bokemeyer, R. van Dantzig, J.F.W. Jansen, B. Kotlinski, M.J.A. de Voigt, J. Van Klinken, *Phys. Lett.* **B180**, 4 (1986).
[25] I.Pomeranchuk, I.Smorodinsky, *J. Phys. (U.S.S.R.)* **9**, 97 (1945).
[26] G.Soff, B.Müller, J.Rafelski, *Z. Naturforsch.* **29A**, 1267 (1974).
[27] B. Müller,J. Rafelski, W.Greiner, *Phys. Lett.* **47B**, 5 (1973).
[28] G. Soff, B. Müller, *Z. Phys.* **A288**, 243 (1977).
[29] B. Müller, G. Soff, W. Greiner, V. Causescu, *Z. Phys.* **A285**, 27 (1978).
[30] B. Müller, J. Reinhard, W. Greiner, G. Soff, *Z.Phys* **A311**, 151 (1983).
[31] E. Kankeleit, *Nukleonika* **25**, 253 (1980).
[32] H.Backe in *Tendances Actuelles en Physique Atomique*, ed. G. Grynberg and R. Stora, Elsevier, Amsterdam 1984, p.699.
[33] P. Armbruster, P. Kienle, *Z. Phys.* **A291**, 399 (1979).
[34] J.S. Greenberg, H. Bokemeyer, H. Emling,E. Grosse, D. Schwalm, F. Bosch, *Phys. Rev. Lett.* **39**, 1404 (1977).
[35] D. Liesen, *Comments At. Mol. Phys.* **12**, 39 (1982).
[36] C. Kozhuharov, P. Kienle, D.H. Jakubassa, M. Kleber, *Phys. Rev. Lett.* **39**, 540 (1977).
[37] C. Kozhuharov, *δ-Ray Spectroscopy of Quasi-Atoms* in Quantum Electrodynamics of Strong Fields, ed. W. Greiner, Plenum Publishing Corporation, 1983, p.317.
[38] H. Backe, L. Handschug, F. Hessberger, E. Kankeleit, F. Weik, R. Willwater, H. Bokemeyer, P. Vincent, Y. Nakayama, J.S. Greenberg, *Phys. Rev. Lett.* **40**, 1443 (1978).
[39] C. Kozhuharov, P. Kienle, E. Berdermann, H. Bokemeyer, J.S. Greenberg, Y. Nakayama, P. Vincent, H. Backe, L. Handschug, E. Kankeleit, *Phys. Rev. Lett.* **42**, 376 (1979).
[40] J. Reinhardt, U. Müller, B. Müller, W. Greiner, *Zeit. Phys.* **A303**, 173 (1981).
[41] E. Kankeleit, U. Gollerthan, G. Klotz, M. Kollatz, M. Krämer, R. Krieg, U. Meyer, H. Oeschler, P. Senger, *Nucl. Instr. Meth.* **A234**, 81 (1985).
[42] M. Rhein, R. Barth, E. Ditzel, H. Feldmeier, E. Kankeleit, V. Lips, C. Müntz, W. Nörenberg, H. Oeschler, A. Piechaczek, I. Schoh, *Phys. Rev. Lett.* **69/9**, 1340 (1992).
[43] R. Bär, A. Bałanda, J. Baumann, W. Berg, K. Bethge, H. Bokemeyer, H. Folger, O. Fröhlich, R. Ganz, O. Hartung, M. Samek, P. Salabura, W. Schön, D. Schwalm, K. Stiebing, P. Thee, E. Berdermann, F. Heine, S. Heinz, O. Joeres, P. Kienle, I. Koenig, W. Koenig, C. Kozhuharov, U. Leinberger, A. Schröter, H. Tsertos, *Nucl. Phys.* **A583**, 237 (1995).
[44] J. Schweppe, PhD Thesis, Yale University (1985).
[45] A. Gruppe, Thesis, University Frankfurt (1985).

[46] W.E. Meyerhof, R. Anholt, *Phys. Lett.* **69B**, 41 (1977).
[47] K. Sakaguchi, Ph.D. Thesis, Frankfurt/M University (1990); GSI-report-90-05 (1990).
[48] M.J. Rhodes-Brown, V.E. Oberacker, M. Seiwert, W. Greiner, *Z. Phys.* **A310**, 287 (1983); M. Seiwert, J.A. Maruhn, W. Greiner, J. Friedrich, *Z. Phys.* **A321**, 653 (1985).
[49] H. Tsertos, F. Bosch, P. Kienle, W. Koenig, C. Kozhuharov, E. Berdermann, S. Huchler, W. Wagner, *Phys. Lett.* **B162**, 273 (1985).
[50] K. Sakakgutchi *et al.*, to be published.
[51] P. Schlüter, G.Soff, W.Greiner, *Atom. Data and Nucl. Data Tables* **24**, 509 (1979).
[52] P. Schlüter, G.Soff, W.Greiner, *Phys. Rep* **75**, 328 (1981).
[53] R. Liotta, R.A. Sorensen, *Nucl. Phys.* **A297**, 136 (1978).
[54] R.D. Peccei, H.R. Quinn, *Phys. Rev.* **D16**, 1791 (1977).
[55] J. van Klinken, W.J. Meyering, F.W.N. de Boer, S.J. Schaafsma, V.A. Wichers, S.Y. van der Werf, G.C.Th. Wierda, H.W. Wilschut, H. Bokemeyer, *Phys. Lett.* **B205**, 223 (1988).
[56] J. van Klinken, F. Bosch, U. Kneissl, E. Lorentz, J. Reinhard, K. Schreckenbach, in *Test of Fundamental laws in Physics* ed. O. Fackler, J. Tran Than Von, Editions Frontieres, Gif-sur Yvette, France 1989, p.147.
[57] J.van Klinken, A. Bałanda, J.M. Hoogduin, H. Kaper, W.J. Meyering, H. Bokemeyer, F.W.N. de Boer, D. Kraft, K.E. Stiebing, *Nucl. Instr. Meth.* **A320**, 508 (1992).
[58] H. Tsertos, P. Kienle, S.M. Judge, K. Schreckenbach, *Phys. Lett.* **B266**, 259 (1991).
[59] M. Davier, H. Nguyen Ngoc, *Phys. Lett.*, **B229**, 150 (1989).
[60] G. Wirth W. Brüchle, M. Brügger, F. Wo, K. Sümmerer, F. Funke, J.V. Kratz, M. Lerch, N. Trautmann, *Phys. Lett.* **B177**, 282 (1986).
[61] J.L. Matthews, T.W. Donnelly, E.H. Farhi, L.S. Osborne ed., PANIC XII, Particlles and Nuclei, Proceedings of the Twelfth International Conference on Particles and Nuclei M.I.T., Cambridge, MA, June 25-29, 1990, Special Isuue of *Nucl. Phys.* **A527**, 795c (1991).
[62] M. Samek, R. Bär, A. Bałanda, J. Baumann, W. Berg, K. Bethge, H. Bokemeyer, H. Folger, R. Ganz, O. Hartung, D. Kraft, H. Kaper, P. Salabura, W.Schön, D. Schwalm, K.E. Stiebing, P. Thee, to be published in *Nucl. Instrum. Methods Phys. Res.*
[63] R.R. Betts, *Nucl. Instrum. Methods Phys. Res.* **B43**, 294 (1989).